Application of metallo-supramolecular branched polymer improves particle distribution and orientation in single-particle cryo-EM

Yixin Xu[1], Lang Wang[2], Yuqi Qin[1], Yingyi Zhang[3], Yufeng Wang[2,*], Shangyu Dang[1,4,5,*]

[1]Division of Life Science, The Hong Kong University of Science and Technology, Clear Water Bay, Kowloon, Hong Kong, China

[2]Department of Chemistry, The University of Hong Kong, Hong Kong, China

[3]Biological Cryo-EM Center, The Hong Kong University of Science and Technology, Clear Water Bay, Kowloon, Hong Kong, China

[4]Hong Kong Branch of Southern Marine Science and Engineering Guangdong Laboratory (Guangzhou), The Hong Kong University of Science and Technology, Clear Water Bay, Kowloon, Hong Kong, China

[5]Center of Systems Biology and Human Health, The Hong Kong University of Science and Technology, Clear Water Bay, Kowloon, Hong Kong, China

*Corresponding author

Abstract

Recent technological breakthroughs in single-particle cryo-electron microscopy (cryo-EM) enabled rapid atomic structure determination of biological macromolecules. A major bottleneck in the current single particle cryo-EM pipeline is to prepare good quality frozen cryo-EM grids, which often is a trial-and-error process. Among many issues, preferred particle orientation and sample damaging by air-water interface (AWI) are common problem in practice. Here we reported a method of applying metallo-supramolecular branched polymer (MSBP) in the cryo-sample preparation for high-resolution single-particle cryo-EM. Our data shows that applying MSBP keeps majority of particles away from air-water interface and mitigates preferred orientation, as demonstrated by analysis of both apoferritin and hemagglutinin (HA) trimer. Together, the use of MSBP is a simple method and could be applied to improve particle distribution for high-resolution structure determination using single-particle cryo-EM.

Introduction

Visualization of biological macromolecules at atomic resolution provides valuable information for unravelling the fundamental mechanisms of many biological processes and also for driving the development of drugs for diseases caused by dysfunctional biological macromolecules. Recent technical breakthroughs in single-particle cryo-EM have powered a “resolution revolution” in structural biology by circumventing the major challenges faced when using traditional X-ray crystallography method[1–4]. Despite the advances, there are still some recurring problems limiting the application of cryo-EM. Among these challenges, preparations of cryo-specimen that are suitable for high-resolution 3D reconstruction using single-particle cryo-EM is still a bottleneck in many cases because vitrification of specimen is a delicate process[5]. For some

proteins, this is the most difficult obstacle to overcome, as a large proportion of protein particles tend to be absorbed to the air-water interface (AWI) in grids, which causes particle disruptions and introduce preferred orientations, making high-resolution structural determinations difficult.

Air-water interface is the main factor causing serious problems in sample preparation because the process for particles hitting the AWI is much faster than the vitrification process of specimen by plunge freezing[6]. As a result, the particles adsorbed and trapped in the AWI may partially unfold and cause structural deformation or even denaturation[7]. Another common situation is that the particles on the AWI exhibit strong orientation preference[8]. Insufficient native conformation protein particles in random orientations make reconstructing a reliable three-dimensional structure at high resolution difficult if not impossible[9].

Several methods have been developed to improve particle behavior in vitreous ice. In some cases, adding detergent, like CHPASO, can eliminate particle adsorption to AWI[10]. Coating of cryo-EM grids with a thin layer of graphene materials as supporting film also improves sample quality in vitreous ice[11–13]. Furthermore, effect of AWI can be reduced by using a new rapid plunge-freezing robots, Spotiton, by decreasing the plunge freezing time compared with conventional vitrification devices[14,15]. In addition, collecting tilted images can also address the insignificant preferred orientation problem[16]. However, requirement of special devices or complicated techniques limit the wide application of these methods. Here, we aim to address these problems of AWI by introducing a novel and simple approach from a new perspective.

Metallo-supramolecular polymers are an emerging type of material that combines the advantages of traditional polymers with coordination chemistry. They can be synthesized by simply mixing polymeric ligands with metal ions to realize tailored structures and properties (charges, magnetic and mechanical

properties, etc.)[17–19]. In this work, we built metallo-supramolecular branched polymers (MSBP) as the additive to assist in the single-particle cryo-EM. Polyethylene glycol (PEG) is employed, which has been extensively used in a variety field, including nanotechnology, nanomedicine and electron microscopy due to their biocompatibility and chemical stability at the relevant milieu[20,21]. The MSBP is formed by functionalizing the chain ends of the PEG with bispyridyl ligands and introducing palladium ions (Pd^{2+}) at room temperature (Fig.1a). The system was previously shown to form hyper-branched polymers[22], which may potentially surround and trap the proteins in central of the solution thus protect them from hitting the AWI.

Here we report on the introduction of MSBP in the sample preparation process, which significantly reduces the AWI effect. First, we confirmed that apoferritin prepared using MSBP can achieve a 2.16 Å high resolution by single-particle cryo-EM method. Second, we showed using cryo-ET technique that apoferritin particles with MSBP are uniformly distributed in the central layer of the vitreous ice, avoiding assembling at the AWI observed for apoferritin without MSBP. In addition, we showed that application of MSBP enabled structure determination of hemagglutinin (HA) trimer at 3.19 Å by minimizing preferred orientation problem of HA trimer as previously reported[15]. All these results suggest that applying MSBP is a straightforward and promising method that can improve particle distribution and orientation of cryo-specimen in vitreous ice for single-particle cryo-EM study.

Results

MSBP does not affect the final resolution of apoferritin

To ensure the practicality and biocompatibility of our approach for high-resolution structural determination using single-particle cryo-EM, we prepared cryo-specimen of apoferritin following the standard protocol except adding

MSBP for the data collection and 3D reconstruction. Briefly, apoferritin was mixed with bispyridyl PEG (MW: 5,000 in this study) and palladium nitrate; the mixture was then immediately applied to cryo-grids and incubated for several minutes to allow formation of metallo-supramolecular structure before blotting and plunge freezing (Fig.1b). The concentration of MSBP has been optimized to ensure proper ice thickness and reduce background noise caused by the metallo-supramolecular structure. Although the concentration of the polymer (2 mg/ml) used to form a branched architecture is well below the gel point (about 30 mg/ml), changes of the solution physical properties, especially the viscosity, are obvious (Supplementary video 1). The raw image of apoferritin prepared with MSBP (Fig.1c) shows homogenous and monodisperse apoferritin particles without obvious background noise that may be contributed by the polymer. In addition, the overall ice quality in grids prepared using MSBP is even better than that in grids without application of MSBP (data not shown), indicating that the metallo-supramolecular structures may influence the AWI to improve reproducibility of cryo-grids by generating better vitreous ice. The good particles of apoferritin, sorted out by 2D and 3D classification, were used to generate 3D reconstructions. The final resolution, calculated using gold-standard Fourier shell correlation (FSC), reaches 2.16 Å, very close to Nyquist limit of acquired micrographs (Fig.1d, Supplementary Fig.1). Local resolutions show high qualities that enable the fitting of individual residues from the published structure (PDB:7KOD) to the density map unambiguously (Fig.1e). This result showed that application of MSBP in sample preparation of single-particle cryo-EM can achieve near-atomic resolution of proteins.

To evaluate the possible resolution reduction because of background noise introduced by MSBP, we also collected apoferritin only dataset under the similar setting and performed a systemically comparison with dataset of apoferritin with MSBP applied. The overall resolution of density map for apoferritin with MSBP is lightly (but not significantly) better compared to the one for apoferritin only

(Supplementary Fig. 2). We then studied the relationship between particle number and resolution. For each dataset, particles used for final 3D reconstruction were split into several 50k particle groups randomly and performed 3D refinement with one or combined groups. Consistently, apoferritin with MSBP resolves a slightly higher resolution density map using under the same number of particle (50k, 100k, 150k), further prove introduction of MSBP has almost no effect on final resolution (Supplementary Fig. 2a). Surprisingly, when we performed contrast transfer function (CTF) refinement (global and local), the improvement for apoferritin with MSBP is much larger than apoferritin only, contributed mainly by local CTF refinement (Supplementary Fig. 2b). Although further evaluation needs to be done, MSBP may benefit the final map quality by providing a better ice quality with more evenly distributed ice thickness. One possible explanation is that MSBP pushed most of the particles into the central layer of the vitreous ice, while the majority particles of apoferritin only are attracted into a limited area close to AWI (Fig. 2, Supplementary Fig. 3a, b). So the defocus of these particles from apoferritin with MSBP will be further optimized, consistent with the large defocus changes for these particles (Supplementary Fig. 2c), thus contribute to the significant resolution improvement. Together, our systematical assessment demonstrated application of MSBP will not affect high-resolution structural determination in single-particle cryo-EM.

MSBP improves particle distribution of apoferritin

To further investigate if MSBP can improve particle distribution in vitreous ice by preventing attraction of particles into the AWI during plunge freezing, we applied cryo-ET approach to locate individual particles in vitreous ice[15]. We collected cryo-ET dataset for apoferritin with or without MSBP for comparison (Supplementary Videos 2, 3) and picked individual particles automatically by template-matching from reconstructed tomograms. For apoferritin without

168 MSBP, an abundance of apoferritin particles were trapped in the AWI, and only
169 a small number of particles were found staying in the middle section of the
170 tomogram (Fig.2a, b, Supplementary Fig.3a). In contrast, for apoferritin treated
171 with MSBP, particles were distributed uniformly throughout the vitreous ice layer
172 with few particles appearing at the AWI (Fig.2c, d, Supplementary Fig. 3b).
173 These distinct particle distributions are more obvious when compared in side
174 (Y-Z) views of the tomograms (Supplementary Fig.4a, b). Also, the obvious air-
175 water interfaces, indicated by the big ice contaminations, shown a thinner ice
176 layer for sample treated with MSBP. We also collected and analyzed cryo-ET
177 datasets of apoferritin treated with PEG or palladium nitrate only, both showing
178 similar particle distribution as the dataset of apoferritin only (Supplementary
179 Fig.3d, e, Supplementary Fig.4d, e). All these results showed that application
180 of MSBP improves particle distribution in an even thinner vitreous ice by
181 keeping particles away from AWI.

182 **MSBP alleviates preferential orientations**

183 We investigated whether particle orientations in vitreous ice are also changed
184 by keeping away from AWI. To test this hypothesis, we collected and analyzed
185 single-particle cryo-EM datasets for hemagglutinin trimer treated with or without
186 MSBP. Consistent to previous studies[15,23], the cryo-EM density map
187 reconstructed using HA trimer only dataset showed distorted feature, indicating
188 severe preferred orientation problem of the data. In contrast, application of
189 MSBP to HA trimer generated a high-resolution map at 3.19 Å that can fit the
190 structure (PDB: 6WXB) very well (Fig.3a, Supplementary Fig.5a, b). To evaluate
191 the map quality, we performed directional FSC (dFSC) analysis for both maps
192 of HA trimer reconstructed from dataset with and without MSBP. For HA trimer
193 only, dFSC showed a wider resolution distribution, suggesting some views were
194 missing in particles used for final reconstruction. For HA trimer with MSBP, a
195 more concentrated resolution distribution of dFSC curves indicated particles

used for final reconstruction were almost equally distributed in different angular directions. This result further confirmed that preferred orientation problem of HA particles in vitreous ice is minimized by introducing MBSP in cryo-sample preparation.

2D classifications were also performed to analyze angular distribution of HA particles in vitreous ice. 2D averages of HA trimer particles showed three distinct orientations: top view, side view, and tilted view (Supplementary Fig.5c, d). We then calculated the number of particles grouped into each of these three categories for the two respective datasets (Fig.3c). The dataset of HA trimer without MSBP exhibited an obvious preferred orientation problem, with more than 50% of particles oriented in top views while only about 13% particles showing typical side views, consistent with previous studies[15,24]. For HA trimer treated with MSBP, the proportion of particles representing top views decreased dramatically (from 57.4% to 23.9%), while particles from both side and tilted views increased correspondingly. It is also worth noting that particles are almost proportionately distributed into three different views in dataset of HA trimer treated with MSBP. 2D averages of top or side views both contain about 30% of total particles, while more than 40% particles are presented as tilted views, the largest category in this dataset. Comparing the statistics of the two HA datasets under different conditions clearly shows that the application of MSBP can alleviate the preferred orientation problem of HA trimmer by protecting particles from AWI such that particles can rotate and distribute more freely in vitreous ice.

Conclusion and Discussion

In summary, we developed a simple and promising method to improve particle behavior in vitreous ice by applying the MSBP for high-resolution single-particle cryo-EM structure determination. We have shown that involvement of MSBP in cryo-specimen preparation not only reduce particles trapped at AWI, but also

alleviate the preferred orientation problem by producing more randomly distributed particles in vitreous ice. Although further investigation need to be performed, trapping particles away from AWI by MSBP may also benefit proteins from denature or partial denature, which is usually caused by adsorption of particles into AWI[25]. In addition to other reported methods such as modification of cryo-grids with graphene oxide, the simplicity of our approach provides an alternative strategy to optimize cryo-sample preparation conditions for challenging protein complexes that do not behave optimally on holey carbon girds.

The PEG-based polymer have many applications in the biology field, such as facilitating cytoskeletal organization of osteoblasts in bone tissue engineering[26] and inhibition of cell migration[27]. MSBP in this study consists of chain-end-modified PEG and palladium ions. PEG has been proven a biological friendly reagent and rarely introduce artificial structures. There are also some papers using photoaffinity palladium reagents to study protein-protein interactions[28]. All these information indicates MSBP is biocompatible. Although the probability is very small, more studies need to be performed to see if MSBP would cause protein damage or change protein structures in future.

As far as we know, this is the first report of applying MSBP for sample preparations in cryo-EM study. Interestingly, we observed that in the air-water interfaces of cryo-grid prepared using MSBP, plenty of uniformly arranged small polymeric particles formed a network, which seem to shield protein particles away from the AWI (Supplementary Video 3, 4, Supplementary Fig.3b, c, Supplementary Fig.4b, c). We did not observe similar networks in cryo-grids without addition of MSBP (Supplementary Video 2, Supplementary Fig.3a, 4a), suggesting the network is formed by the MSBP. We hypothesize that the presence of the branched polymer in the solution may change the local viscosity of the solution[29] and retards the adsorption rate of the protein into the AWI

252 (Supplementary Video 1). Although different to high-speed freezing[15], our
253 method shares the same idea to reduce spread rate of particles to AWI by
254 increasing solution viscosity. Alternatively, the MSBP may be recruited to the
255 AWI with a speed faster than protein particles and form a network that protects
256 particles from adsorption into AWI. The exact mechanism of how MSBP
257 facilitates to redistribute protein complexes is yet to be determined.

258 Although application of MSBP for cryo-sample preparation would introduce
259 some background noise in collected micrographs, the final 3D reconstruction is
260 affected little since these random background noises could be averaged out by
261 data processing. For protein with large mass, like apoferritin in this study, the
262 3D reconstruction actually is benefited by application of MSBP, giving a higher
263 reported resolution for cryo-EM density map generated using the same number
264 of particles (Supplementary Fig.2a, b), which further suggested attaching of
265 protein particles into AWI may cause instability or even damage of the protein.
266 For proteins with small mass like HA trimer, the resolution is affected by these
267 background noises, due to a lower signal-to-noise ratio (SNR) in micrographs
268 with application of MSBP. However, this problem could be compensated by
269 collecting a larger set of particles, in which way to strengthen SNR and further
270 improve resolution. Using a larger dataset for HA with MSBP, we finally obtained
271 a high quality cryo-EM density map for structural analysis (Fig.3a,
272 Supplementary Fig.5a, b).

273 In some cases, addition of detergent can also improve particle distribution in
274 vitreous ice[10]. Systematical study shown nonionic and zwitterionic but not ionic
275 detergent could separate protein particles from AWI[30]. Specially, addition of low
276 concentration cetyltrimethylammonium bromide (CTAB), a cationic surfactant,
277 to cryo-sample of HA trimer could provide more evenly distributed protein
278 particles in vitreous ice to facilitate high-resolution structure determination,
279 although most of the protein particles were still absorbed to AWI[30]. Different

280 from surfactant that is favored to attach in AWI and expose their hydrophobic
281 tail outside, MSBP is highly hydrophilic and has a more random distribution in
282 solution. In addition, MSBP increases viscosity of the solution, which might be
283 one of the reasons to provide a random distribution of protein particles inside.
284 Furthermore, addition of detergent to improve protein angular distribution is also
285 a trial-and-error process. For other proteins than HA trimer, introducing of CTAB
286 limited particle distribution in a narrower angular range than that without CTAB[30].
287 Comparison of particle distribution for HA trimer with or without MSBP further
288 demonstrated our method can facilitate an evenly distribution of protein
289 particles in vitreous ice with a different mechanism than that using surfactant
290 (Supplementary Fig.6).

291 Protecting biological macromolecules from AWI is a reasonable way to avoid
292 recurring problems in cryo-specimen preparation for single particle cryo-EM
293 studies. Previously, different methods have been developed to address AWI
294 problem, including tracking proteins away from AWI using graphene oxide
295 based substrate approach[12], changing protein surface properties by
296 PEGylation[31,32], and so on. In a long term, we aim to develop a universal
297 method that can be applied to most of the biological macromolecules, despite
298 difference they may have. In this study, we introduced MSBP in cryo-sample
299 preparation to reduce the probability of particle interacting with AWI. Although
300 the concentration we used is quite lower than the required concentration for gel
301 formation, the physical properties of the solution has changed obviously
302 (Supplementary Video 1). Following this idea, if we can find some reagents that
303 could form biological compatible branched structures or network (either
304 chemical or protein network) at a lower concentration, their ability of trapping
305 protein particles away from AWI would increase dramatically compared to
306 MSBP. These kinds of network are more ideal for application to sample
307 preparation in single particle cryo-EM to minimize AWI effects. Inside of the
308 network, particles are surrounded randomly, thus the potential noise introduced

by network certainly could be averaged out during data processing and would affect little of the final map quality. We are looking for the network with above mentioned properties, which to be applied in cryo-sample preparation process to facilitate the structural determination using single particle cryo-EM.

Briefly, our approach described here will help cryo-sample preparation by diminishing AWI effects and eventually contribute to resolution improvement with a wide applicable potential, eventually benefitting the whole cryo-EM community.

Figure Legend

Fig.1 Apoferritin, with application of metallo-supramolecular branched polymer (MSBP) in sample preparation, can achieve a high resolution. (a) Schematic diagram of local structure of MSBP in solution. Branched polymers are formed in solution. **(b)** Workflow for preparation of apoferritin cryo-specimen with MSBP. Apoferritin, mixed with 2 mg/mL modified PEG5000 and 0.24 mg/mL $Pd(NO_3)_2$, was loaded onto the holey carbon grid. **(c)** A representative cryo-micrograph of apoferritin prepared with MSBP. Fourier transformation of the micrograph is also shown in left bottom with Thon rings extending to 3Å. **(d)** 3D reconstruction of apoferritin prepared with MSBP at 2.16-Å resolution. **(e)** Representative cryo-EM densities of one α helix of apoferritin. The density is shown as grey mesh and the corresponding structural model (PDB: 7KOD) in blue with side chains of residues depicted to demonstrate the quality of the map.

Fig.2 Particle distribution of apoferritin in vitreous ice layer analyzed by cryo-ET. (a) Localization of particles from apoferritin without MSBP grid shown most of particles were absorbed to the top air-water interface. Particles were picked by template matching in Dynamo. **(b)** Particle distribution of apoferritin without MSBP in three layers along the Z axis of the tomogram. **(c)** Localization

of particles from apoferritin with MSBP grid shown more uniform distribution. Particles were picked by template matching in Dynamo. **(d)** Particle distribution of apoferritin with MSBP in three layers along the Z axis of the tomogram. Regular arranged small particles are observed in two air-water interfaces.

Fig.3 Cryo-EM analysis of hemagglutinin (HA) trimer. (a) Local resolution of HA trimer in two different views, as estimated by cryoSPARC and shown with pseudo-color representation of resolution. **(b)** dFSC from different Fourier cones for HA with or without MSBP. Each curve indicates a different direction. **(c)** Statistics of HA trimer particles in three different views. Obviously, top views are the preferred orientation of HA trimer without MSBP. The proportions of the side views and tilted views of HA trimer with MSBP increased significantly.

Materials and Methods

Synthesis of bispyridyl polyethylene glycol (bispyridyl PEG).

The synthesis of succinylated bispyridyl ligand L-COOH.

4-((3,5-di(pyridin-4-yl)benzyl)oxy)-4-oxobutanoic acid. To a 50 mL Schlenk flask equipped with a magnetic stirring bar were added [3,5-di(pyridine-4-yl)phenyl]methanol (2.5 g, 9.54 mmol), succinic anhydride (1.15 g, 11.5 mmol), and 4-dimethylaminopyridine (1.4 g, 11.5 mmol). The flask was capped with a septum and evacuated and refilled with nitrogen three times. To the flask via syringe were added 30 mL anhydrous dichloromethane (DCM) under nitrogen. The flask was placed at room temperature for overnight. The contents of the flask was concentrated via rotary evaporation to give crude product which was subjected to chromatography on silica gel (CH_2CL_2/MeOH/CH_3COOH step gradient, 10:0:0→97:1.5:1.5→94:3:3); the fractions containing desired product were combined, concentrated to yield a light yellow solid. The product was

362 further purified by washing with de-ionized water for 8-10 times to remove the
363 excess of succinic acid and acetic acid, and dried by lyophilization to give off-
364 white powdery solid. HRMS (EI): calcd. for $C_{21}H_{18}O_4N_2$, most abundant m/z =
365 362.1261; found, 362.1270.

366 Polyethylene glycol were then coupled with the succinylated ligand via a DIC
367 (*N,N'*-diisopropylcarbodiimide) mediating coupling protocol. Typically, to a 25
368 mL Schlenk flask equipped with a magnetic stirring bar were added the OH-
369 PEG_{5k}-OH (300 mg, 0.06 mmol), the succinylated bispyridyl ligand (87 mg, 0.24
370 mmol), and 4-dimethylaminopyridine (8.0 mg, 0.065 mmol), the flask was
371 capped with a septum and evacuated and refilled with nitrogen three times. To
372 the flask via syringe were added 10 mL anhydrous dichloromethane (DCM) and
373 2 mL anhydrous *N,N*-dimethylformamide (DMF) under nitrogen. DIC (80 μL,
374 0.52 mmol) was then added under nitrogen. The flask was placed at room
375 temperature for 48 h. The crude product was purified by prep-HPLC, eluent flow
376 rate was 10 mL/min, and the eluent composition consisted of mixtures of
377 ultrapure water and HPLC grade acetonitrile. The eluent gradient consisted of
378 a linear ramp from 35% to 80% acetonitrile during 0-30 min, followed by a ramp
379 to 95% acetonitrile during 30-45 min. Fractions containing the product were
380 combined, froze and lyophilized.

381 **Sample preparation**

382 Cryo-grids preparation of apoferritin

383 The mouse heavy chain apoferritin sample was expressed and purified
384 following the standard protocol[33].

385 Bispyridyl PEG-5k (L-PEG-L) was dissolved to 50 mg/ml in H_2O, and $Pd(NO_3)_2$
386 was dissolved to 5 mg/ml in DMSO as stock solution. The stock solution was
387 further diluted to the indicated concentrations using buffer the same as proteins

before mixing with protein sample. The holey carbon grids (Quantifoil 300 mesh Cu R1.2/1.3) were glow-discharged for 30s before application of all cryo-specimen used in this study.

For single-particle cryo-EM grid, 1 μL apoferritin (2 mg/ml), 1 μL L-PEG-L (6 mg/ml) and 1 μL $Pd(NO_3)_2$ (0.72 mg/ml) were well mixed and applied to holey carbon grids. After 60 s incubation on the grids at 22 °C under 100% humanity, the grids were blotted with filter paper (TED PELLA 595) for 6 s and plunge-frozen into liquid ethane cooled by liquid nitrogen using a FEI MarkIV Vitrobot. To prepare cryo-grids for cryo-ET studies, a similar protocol was used except gold tracers (BSA tracer Conventional, 10 nm, AURION) were mixed with sample before loading to the grids. The MSBP grids were prepared by replacing apoferritin by buffer.

To prepare the cryo-grid of apoferritin without MSBP, 3 μL apoferritin (0.67 mg/ml) was loaded on the holey carbon grids (Quantifoil 400 mesh Cu R1.2/1.3) which was glow discharged for 30s. The grid was plunge-frozen by the same protocol.

Cryo-grids preparation of hemagglutinin

The HA trimer recombinant protein purchased from MyBioSource (Catalog number MBS434205) was dissolved in PBS buffer to indicated concentration. To prepare HA trimer only grid for single-particle cryo-EM studies, 3 μL HA trimer (0.75 mg/ml) was applied to holey carbon grid (Quantifoil 400 mesh Au R1.2/1.3) which was glow discharged 30 s at 15 mA. After 30 s incubation at 22 °C under 100% humanity, the grid was blotted with filter paper (TED PELLA 595) for 4 s and plunge-frozen into liquid ethane cooled by liquid nitrogen. To prepare HA trimer with MSBP grid for single-particle cryo-EM studies, 3 μL HA trimer (1 mg/ml), 0.5 μL L-PEG-L (8 mg/ml) and 0.5 μL $Pd(NO_3)_2$ (1 mg/ml) was applied to holey carbon grid (Quantifoil 200 mesh Cu R2/2) which was glow

415 discharged 45 s at 15 mA. After 120 s incubation at 22 °C under 100% humanity,
416 the grid was blotted with filter paper (TED PELLA 595) for 7 s and plunge-frozen
417 into liquid ethane cooled by liquid nitrogen.

418 To prepare HA trimer only grid for cryo-ET studies, 3 μL HA trimer (0.75 mg/ml)
419 was applied to holey carbon grid (Quantifoil 400 mesh Cu R1.2/1.3) which was
420 glow discharged 30 s at 15 mA. After 60 s incubation at 22 °C under 100%
421 humanity, the grid was blotted with filter paper (TED PELLA 595) for 4 s and
422 plunge-frozen into liquid ethane cooled by liquid nitrogen. To prepare HA trimer
423 with MSBP grid for cryo-ET studies, a similar protocol was used except 0.5 μL
424 L-PEG-L (4 mg/ml) and 0.5 μL $Pd(NO_3)_2$ (0.5 mg/ml) were mixed with 3 μL HA
425 trimer (1 mg/ml) for grid loading.

426

427 **Data collection and processing**

428 All cryo-EM data collection was done with a FEI Titan Krios G3i electron
429 microscope (Thermo Fisher Scientific) equipped with a high-brightness field
430 emission gun operated at 300 kV.

431 For single-particle cryo-EM, images were recorded with a K3 Summit direct
432 electron detector (Gatan) using EPU[34] in counting mode at a calibrated
433 magnification of 81,000X (1.06 Å physical pixel size). The slit width of the Gatan
434 Imaging Filter (GIF) Bio Quantum was set to 20 eV. 2090 micrographs were
435 collected over 8 s with 7.13 $e^-/Å^2/s$ dose rate for the dataset of apoferritin. 1587
436 micrographs were collected over 8 s with 7.13 $e^-/Å^2/s$ dose rate for the dataset
437 of apoferritin with MSBP. 576 micrographs were collected over 5 s with 10.35
438 $e^-/Å^2/s$ dose rate for the dataset of HA trimer. 3861 micrographs were collected
439 over 4.5 s with 11.31 $e^-/Å^2/s$ dose rate for the dataset of HA trimer with MSBP.
440 All micrographs with 40 frames were collected with defocus values from
441 −2.5 μm to −1.3 μm.

442 Drift correction of the micrographs was performed using MotionCor2[35]. Motion-
443 corrected sums without does-weighting were used for contrast transfer function
444 (CTF) estimation with GCTF[36]. Motion-corrected sums with does-weighting
445 were used for all other image processing. Particles picked by Gautomatch
446 (https://www.mrclmb.cam.ac.uk/kzhang/Gautomatch/) were extracted by
447 RELION[37] and then imported into CryoSPARC[38] for further processing. The
448 initial model was generated using ab initio reconstruction. Well-sorted particles
449 by iterative 2D classification and heterogeneous refinement were finally
450 subjected to homogenous and non-uniform refinement to generate the final
451 maps. CTF refinement was performed to further improve the final resolution.
452 Detailed information of data processing of apoferritin can be found in
453 Supplementary Fig.1.

454 Similar approaches were used to process HA trimer dataset. In this case, 2D
455 averages were used to evaluate the angular distribution of the particles. The
456 final 2D classification results for HA trimer with or without MSBP can be found
457 in Supplementary Fig.5 c, d. 2D templates of HA trimer with MSBP generated
458 by a 3D density map were used to pick more particles from images for further
459 processing to generate final map. Detailed information of data processing of HA
460 trimer with MSBP can be found in Supplementary Fig.5a.

461 For cryo-ET data of apoferritin, tilt series from -60° to 60° with 3° increments,
462 were collected with a K3 Summit direct electron detector (Gatan) using
463 Tomography (Thermo Fisher Scientific)[39] in counting mode at a calibrated
464 magnification of 42,000X (2.09 Å physical pixel size). A total dose of 2.16 $e^{-}/Å^2$
465 (for apoferritin only and MSBP only), 2.92 $e^{-}/Å^2$ (for apoferritin with MSBP) and
466 2.72 $e^{-}/Å^2$ (for apoferritin with PEG and apoferritin with $Pd(NO_3)_2$) was used to
467 expose every micrograph for around 1s (4 frames per image) with a defocus
468 near -4 μm.

469 For cryo-ET data of HA trimer, tilt series from -45° to 45° with 3° increments,

470 were collected with a K3 Summit direct electron detector (Gatan) using
471 Tomography (Thermo Fisher Scientific)[39] in counting mode at a calibrated
472 magnification of 53,000X (1.7 Å physical pixel size). A total dose of 4.19 $e^{-}/Å^{2}$
473 (for HA trimer with and without MSBP) was used to expose every micrograph
474 for around 1.8 s (6 frames per image) with a defocus near -5 μm.

475 The micrographs were aligned by MotionCor2 without CTF correction. The tilt
476 series were aligned based on gold fiducials by making seed model manually in
477 Etomo[40]. After the generation of tomograms, the particles were picked by
478 template matching in Dynamo[41].

479

480

481

482 **References**

483 1. Wu, M. & Lander, G. C. Present and Emerging Methodologies in Cryo-
484 EM Single-Particle Analysis. *Biophysical Journal* **0**, (2020).

485 2. Nakane, T. *et al.* Single-particle cryo-EM at atomic resolution. *Nature* **587**,
486 152–156 (2020).

487 3. Yip, K. M., Fischer, N., Paknia, E., Chari, A. & Stark, H. Atomic-resolution
488 protein structure determination by cryo-EM. *Nature* **587**, 157–161 (2020).

489 4. Cheng, Y. Single-particle cryo-EM—How did it get here and where will it
490 go. *Science (80-.).* **361**, 876–880 (2018).

491 5. Passmore, L. A. & Russo, C. J. *Specimen Preparation for High-*
492 *Resolution Cryo-EM*. *Methods in Enzymology* **579**, (Elsevier Inc., 2016).

493 6. Lyumkis, D. Challenges and opportunities in cryo-EM single-particle
494 analysis. *J. Biol. Chem.* **294**, 5181–5197 (2019).

495 7. Glaeser, R. M. Proteins, interfaces, and cryo-EM grids. *Curr. Opin.*
496 *Colloid Interface Sci.* **34**, 1–8 (2018).

497 8. Drulyte, I. *et al.* Approaches to altering particle distributions in cryo-
498 electron microscopy sample preparation. *Acta Crystallogr. Sect. D Struct.*
499 *Biol.* **74**, 560–571 (2018).

500 9. Lyumkis, D. Challenges and opportunities in cryo-EM single-particle
501 analysis. *J. Biol. Chem.* **294**, 5181–5197 (2019).

502 10. Chen, J., Noble, A. J., Kang, J. Y. & Darst, S. A. Eliminating effects of
503 particle adsorption to the air/water interface in single-particle cryo-
504 electron microscopy: Bacterial RNA polymerase and CHAPSO. *J. Struct.*
505 *Biol. X* **1**, 100005 (2019).

506 11. Han, Y. *et al.* High-yield monolayer graphene grids for near-atomic
507 resolution cryoelectron microscopy. *Proc. Natl. Acad. Sci. U. S. A.* **117**,
508 1009–1014 (2020).

509 12. Wang, F. *et al.* Amino and PEG-amino graphene oxide grids enrich and
510 protect samples for high-resolution single particle cryo-electron
511 microscopy. *J. Struct. Biol.* **209**, 107437 (2020).

512 13. Liu, N. *et al.* Bioactive Functionalized Monolayer Graphene for High-
513 Resolution Cryo-Electron Microscopy. *J. Am. Chem. Soc.* **141**, 4016–
514 4025 (2019).

515 14. Jain, T., Sheehan, P., Crum, J., Carragher, B. & Potter, C. S. Spotiton: A
516 prototype for an integrated inkjet dispense and vitrification system for
517 cryo-TEM. *J. Struct. Biol.* **179**, 68–75 (2012).

518 15. Noble, A. J. *et al.* Reducing effects of particle adsorption to the air–water
519 interface in cryo-EM. *Nat. Methods* **15**, 793–795 (2018).

520 16. Zi Tan, Y. *et al.* Addressing preferred specimen orientation in single-
521 particle cryo-EMthrough tilting. *Nat. Methods* **14**, 793–796 (2017).

522 17. Beck, J. B., Ineman, J. M. & Rowan, S. J. Metal/Ligand-Induced
523 Formation of Metallo-Supramolecular Polymers. *Macromolecules* **38**,
524 5060–5068 (2005).

525 18. Winter, A. & Schubert, U. S. Synthesis and characterization of metallo-
526 supramolecular polymers. *Chem. Soc. Rev.* **45**, 5311–5357 (2016).

527 19. Whittell, G. R., Hager, M. D., Schubert, U. S. & Manners, I. Functional
528 soft materials from metallopolymers and metallosupramolecular
529 polymers. *Nature Materials* **10**, 176–188 (2011).

530 20. Zalipsky, S. & Harris, J. M. Introduction to Chemistry and Biological

Applications of Poly(ethylene glycol). *ACS Symp. Ser.* **680**, 1–13 (1997).

21. Wolosewick, J. J. The application of polyethylene glycol (PEG) to electron microscopy. *J. Cell Biol.* **86**, 675–681 (1980).

22. Zhukhovitskiy, A. V. *et al.* Highly branched and loop-rich gels via formation of metal–organic cages linked by polymers. *Nat. Chem.* **8**, 33–41 (2016).

23. Tan, Y. Z. *et al.* Addressing preferred specimen orientation in single-particle cryo-EM through tilting. *Nat. Methods* **14**, 793–796 (2017).

24. Tan, Y. Z. & Rubinstein, J. L. Through-grid wicking enables high-speed cryoEM specimen preparation. *Acta Crystallogr. Sect. D Struct. Biol.* **76**, 1092–1103 (2020).

25. Klebl, D. P. *et al.* Need for Speed: Examining Protein Behavior during CryoEM Grid Preparation at Different Timescales. *Structure* **28**, 1238-1248.e4 (2020).

26. Burdick, J. A. & Anseth, K. S. Photoencapsulation of osteoblasts in injectable RGD-modified PEG hydrogels for bone tissue engineering. *Biomaterials* **23**, 4315–4323 (2002).

27. Raeber, G. P., Lutolf, M. P. & Hubbell, J. A. Molecularly engineered PEG hydrogels: A novel model system for proteolytically mediated cell migration. *Biophys. J.* **89**, 1374–1388 (2005).

28. Zheng, Q. *et al.* Photoaffinity palladium reagents for capture of protein-protein interactions. *Org. Biomol. Chem.* **17**, 6369–6373 (2019).

29. Yates, C. R. & Hayes, W. Synthesis and applications of hyperbranched polymers. *Eur. Polym. J.* **40**, 1257–1281 (2004).

30. Li, B., Zhu, D., Shi, H. & Zhang, X. Effect of charge on protein preferred

orientation at the air–water interface in cryo-electron microscopy. *J. Struct. Biol.* **213**, 107783 (2021).

31. Zhang, Z., Shigematsu, H., Shimizu, T. & Ohto, U. Improving particle quality in cryo-EM analysis using a PEGylation method. *Structure* (2021). doi:10.1016/J.STR.2021.05.004

32. Wu, X., Cabanos, C. & Rapoport, T. A. Structure of the post-translational protein translocation machinery of the ER membrane. *Nat. 2018 5667742* **566**, 136–139 (2018).

33. Wu, M., Lander, G. C. & Herzik, M. A. Sub-2 Angstrom resolution structure determination using single-particle cryo-EM at 200 keV. *J. Struct. Biol. X* **4**, 100020 (2020).

34. Hillsboro, T. P. EPU Software User ' s Guide.

35. Zheng, S. Q. *et al.* MotionCor2: Anisotropic correction of beam-induced motion for improved cryo-electron microscopy. *Nat. Methods* **14**, 331–332 (2017).

36. Zhang, K. Gctf: Real-time CTF determination and correction. *J. Struct. Biol.* **193**, 1–12 (2016).

37. Zivanov, J., Nakane, T. & Scheres, S. H. W. Estimation of high-order aberrations and anisotropic magnification from cryo-EM data sets in RELION-3.1. *IUCrJ* **7**, 253–267 (2020).

38. Punjani, A., Rubinstein, J. L., Fleet, D. J. & Brubaker, M. A. CryoSPARC: Algorithms for rapid unsupervised cryo-EM structure determination. *Nat. Methods* **14**, 290–296 (2017).

39. Benefits, K. Tomography 5 Software. 3–6

40. Kremer, J. R., Mastronarde, D. N. & McIntosh, J. R. Computer visualization of three-dimensional image data using IMOD. *J. Struct. Biol.* **116**, 71–76 (1996).

41. Castaño-Díez, D., Kudryashev, M., Arheit, M. & Stahlberg, H. Dynamo: A flexible, user-friendly development tool for subtomogram averaging of cryo-EM data in high-performance computing environments. *J. Struct. Biol.* **178**, 139–151 (2012).

Data Availability

Cryo-EM density map of mouse apoferritin has been deposited in the Electron Microscopy Data Bank (accession no. EMD-XXXX). All other data are available from the corresponding authors upon reasonable request.

Acknowledgments

We thank Bik Tye and Yifan Cheng for their critical reading of the manuscript, Masa Kikkawa at University of Tokyo for generously sharing mouse heavy chain apoferritin plasmid with us. We also thank Chunlin He, Zhongguang Yang, and Fei Sun for their helpful discussion in the early stage of this project. All cryo-EM data were collected at the Biological Cryo-EM Center at HKUST, generously supported by a donation from the Lo Kwee Seong Foundation. This project is supported by grants of S.D. from Hong Kong Research Grants Council (ECS26101919, GRF16103321, C7009-20GF, C6001-21EF), the Hong Kong Branch of Southern Marine Science and Engineering Guangdong Laboratory (Guangzhou) (SMSEGL20SC01), Guangdong Natural Science Foundation (GDST21SC04), Shenzhen Science and Technology Innovation Committee (SZ-SZSTI2108) and HKUST start-up and initiation grants. Y.W. acknowledges support from General Research Fund from Hong Kong Research Grants Council (17308518) and Croucher Innovation Award 2019 (Croucher

Foundation, Hong Kong).

Author contributions

Y.X., Y.Q. and S.D. designed and performed single-particle cryo-EM experiments. Y.X., Y.Q. and Y.Z. performed cryo-ET experiments. Y.X. and L.W. prepared specimen using MSBP. S.D. and Y.W. supervised experiments and data analysis. All authors contributed to manuscript preparations.

Competing financial interest

The method applying metallo-supramolecular branched polymer (MSBP) in sample preparation of single particle cryo-electron microscopy (cryo-EM) is described in a provisional patent application.

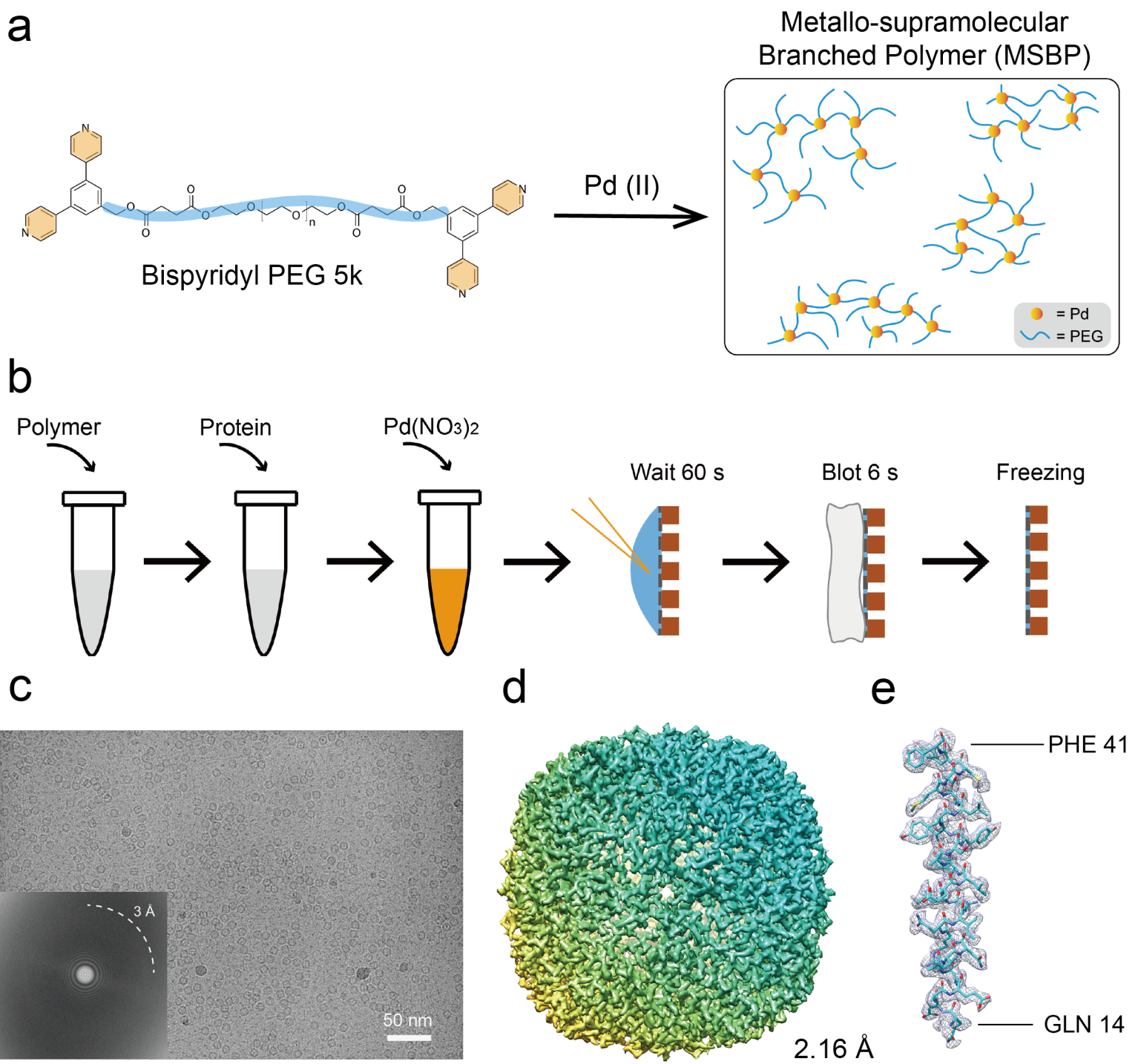
a
Metallo-supramolecular
Branched Polymer (MSBP)
Bispyridyl PEG 5k
Pd (II)
= Pd
= PEG
b
Polymer
Protein
Pd(NO3)2
Wait 60 s
Blot 6 s
Freezing
c
d
e
3 Å
50 nm
2.16 Å
PHE 41
GLN 14

Figure.1

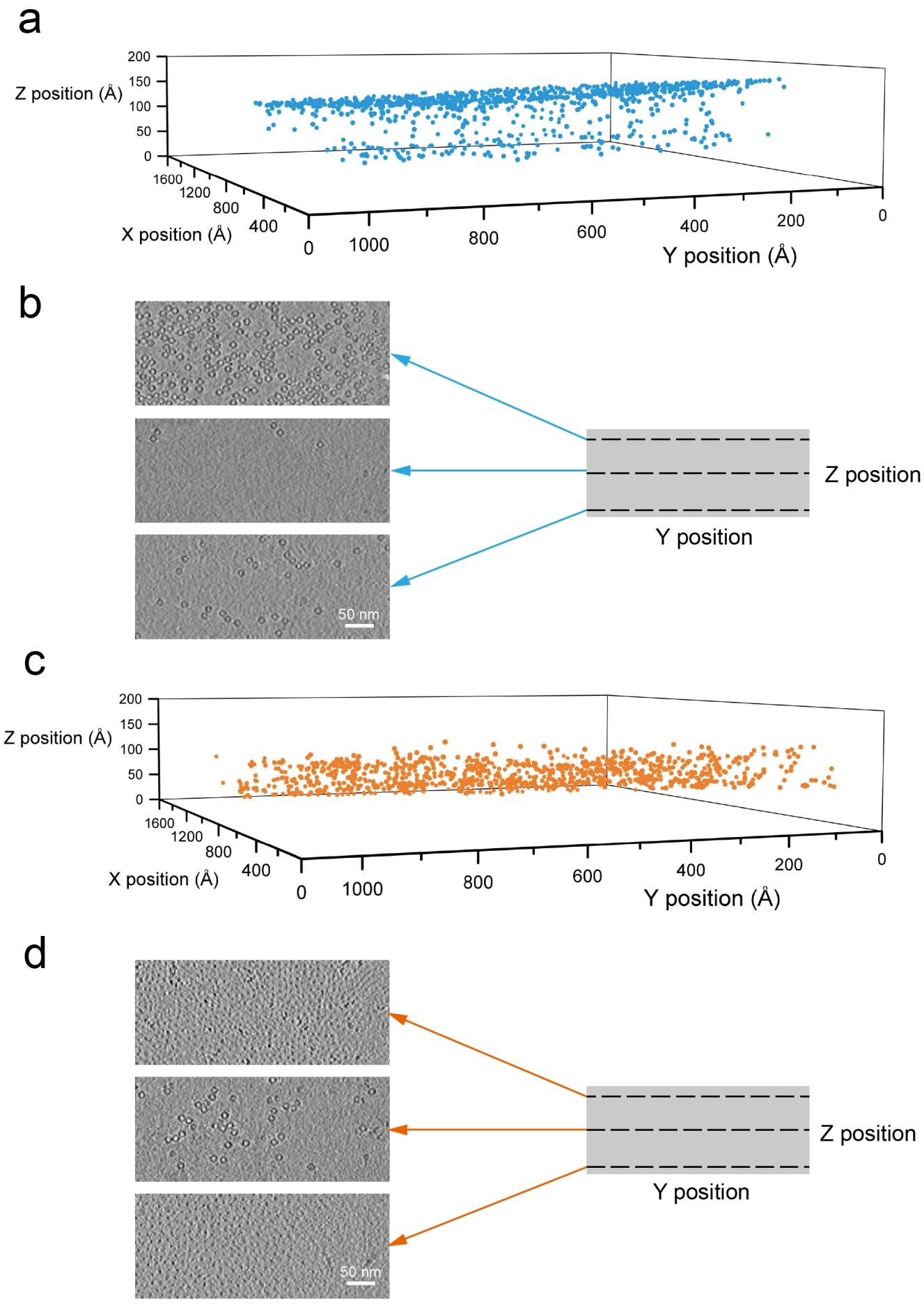
a
Z position (Å)
200
150
100
50
0
1600
1200
800
400
X position (Å)
0
1000
800
600
400
200
0
Y position (Å)
b
Z position
Y position
50 nm
c
Z position (Å)
200
150
100
50
0
1600
1200
800
400
X position (Å)
0
1000
800
600
400
200
0
Y position (Å)
d
Z position
Y position
50 nm

Figure.2

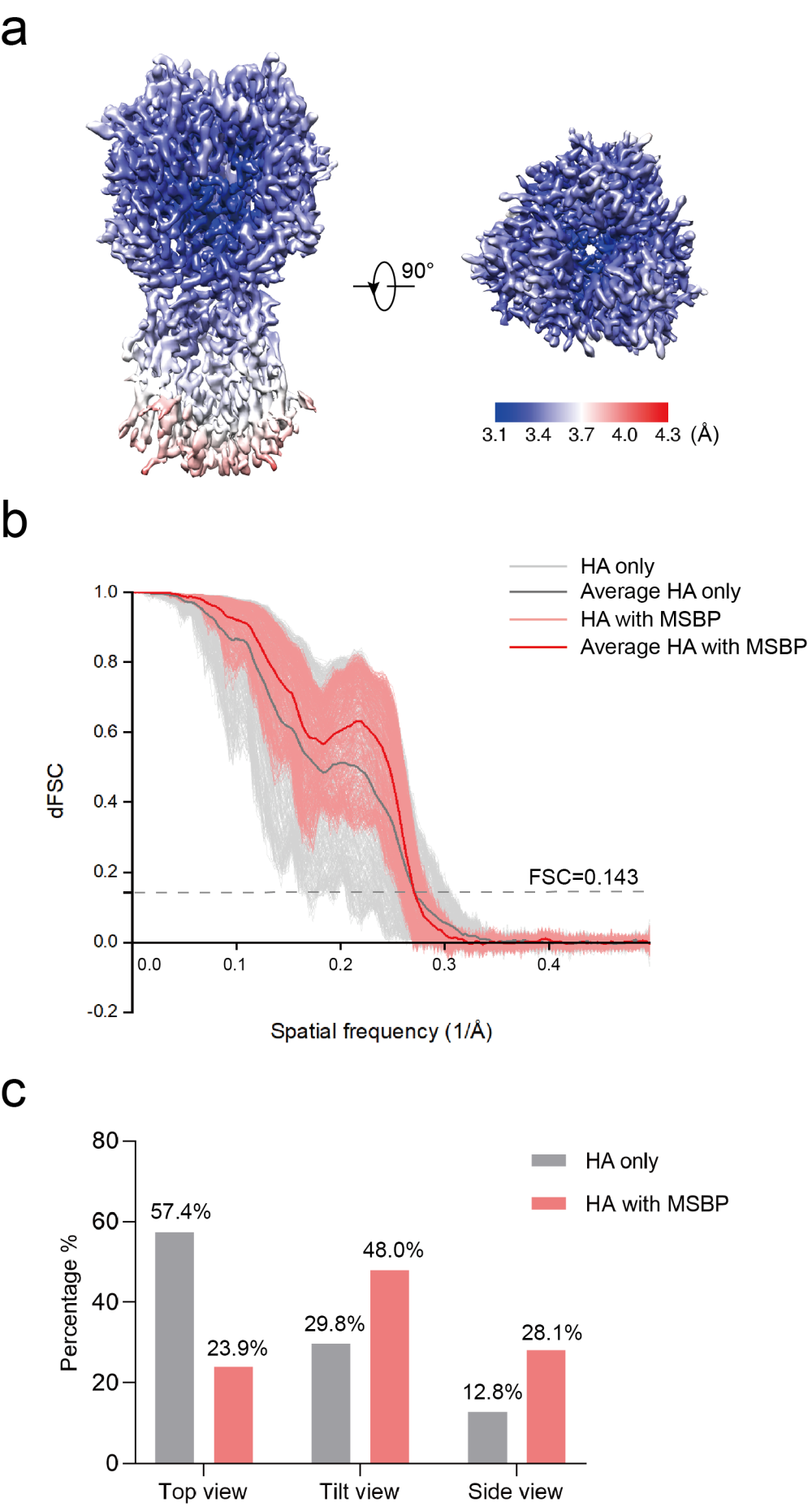
a
90°
3.1 3.4 3.7 4.0 4.3 (Å)
b
HA only
Average HA only
HA with MSBP
Average HA with MSBP
dFSC
1.0
0.8
0.6
0.4
0.2
0.0
-0.2
FSC=0.143
0.0
0.1
0.2
0.3
0.4
Spatial frequency (1/Å)
c
HA only
HA with MSBP
Percentage %
80
60
40
20
0
57.4%
23.9%
29.8%
48.0%
12.8%
28.1%
Top view
Tilt view
Side view

Figure.3